Research Article | Vol. 28, No. 22 / 26 October 2020 / Optics Express 32802
Optics EXPRESS

Comprehensive study of the rapid stressed mirror polishing method for off-axis aspheric SiC thin-plate mirrors

LIQI YI,[1,2] XUEJUN ZHANG,[1,4] HAIFEI HU,[1,3,5] ZHIYU ZHANG,[1] KUO HAI,[1,2] XIAO LUO,[1] AND DONGLIN XUE[1]

[1]*Key Laboratory of Optical System Advanced Manufacturing Technology, Changchun Institute of Optics, Fine Mechanics and Physics, Chinese Academy of Sciences, Changchun, Jilin 130033, China*
[2]*University of Chinese Academy of Sciences, Beijing 100049, China*
[3]*School of Mechanical and Aerospace Engineering, Jilin University, Changchun, Jilin 130022, China*
[4]*zxj@ciomp.ac.cn*
[5]*huhf@ciomp.ac.cn*

Abstract: In this study, the stressed mirror polishing technique is used to perform off-axis aspheric silicon carbide (SiC) mirror full-aperture polishing for the first time. Mechanical and optical parameter analysis methods have been proposed. A medium-diameter off-axis aspheric SiC thin-plate mirror is used as a scaling model for an optical system mirror. A full diameter polishing simulation was completed, and a conceptual design for stress loading equipment is presented. An initial aspheric surface method for stressed mirror polishing of an off-axis aspheric SiC thin-plate mirror, providing a reference for rapid stress mirror polishing of SiC mirrors, is also proposed.

1. Introduction

After the advent of the Keck telescope and other telescopes with 10-m-diameter spliced mirrors, the optical transmission capacity of astronomical observation equipment has increased dramatically. To meet the development needs of astronomy, several countries and regions worldwide have proposed a succession of large-aperture telescope plans, and this has started an era where the apertures of optical astronomical telescopes have been increasing. At present, the Thirty Meter Telescope (TMT) is being developed. The stressed mirror polishing technique [1,2], which uses a large-diameter contact tool to polish off-axis aspherical surfaces, was developed during the construction of spliced segmented mirrors. As the polishing object is converted from an aspherical surface to a spherical surface, large-diameter contact tools can be used to considerably improve the machining efficiency. Compared with the conventional small-area contact tool polishing method that is computer-controlled optical surfacing (CCOS), the method allows high-frequency surface errors to be reduced. At present, this method is generally used to polish the low-expansion glass plate segmented mirror of the primary mirror in large ground-based telescope systems.

In recent years, with the increase in the number of large-scale space-based optical facilities, traditional glass materials have shown many limitations in terms of their mechanical and thermal properties. Additionally, new space materials with better performance have gradually been applied and have replaced traditional glass materials within a certain operating range. SiC is a high-quality space mirror material that has stable chemical properties, high thermal conductivity, a small thermal expansion coefficient, and high specific stiffness. Further, it has been widely used in remote sensing and observation systems for single mirrors. However, SiC is a brittle material with ceramic characteristics. Hence, the main SiC machining techniques are still magnetorheological finishing methods [3,4], small tool manufacturing processes [5], and similar methods. Owing

#405389 https://doi.org/10.1364/OE.405389
Journal © 2020 Received 13 Aug 2020; revised 3 Oct 2020; accepted 4 Oct 2020; published 15 Oct 2020

Optics EXPRESS

to the inherent intermediate frequency oscillations of these sub-aperture machining methods, middle- and high-frequency errors are unavoidable, and the associated small removal volumes and long processing times are not suitable for the rapid manufacturing requirements of large-aperture aspheric mirrors. In particular, with the development of large space-based observation systems, such as geostationary orbit systems, performing in-orbit assembly of large-aperture primary mirrors and finding full-aperture stressed mirror polishing methods for the segmented mirrors are now urgently necessary. However, owing to the high hardness and low removal rate of SiC, numerous factors, including fracture and damage, cause uncertainty in the stressed loading and polishing processes.

Therefore, the Optical Technology Research Center of the Changchun Institute of Optics, Fine Mechanics and Physics (CIOMP) of the Chinese Academy of Sciences established an innovation group for stressed mirror polishing and rapid processing technology development for off-axis aspheric SiC mirrors, and it deployed the resulting research work into this new optical manufacturing technology. The CIOMP, after years of research into SiC materials sintering and improvement and modification of the processing technology, developed monomer SiC off-axis aspheric mirrors with a diameter of 4.03 m in 2017. The monomer off-axis aspheric SiC mirror is used worldwide in space and ground equipment loads. The time is now appropriate for research regarding the suitable rapid processing technology for these spliced segmented mirrors.

This paper describes relatively basic research on stressed mirror polishing and rapid processing methods and the technology of SiC off-axis aspheric thin-plate mirrors, and then it demonstrates the feasibility of applying stressed mirror polishing technology to the rapid production of SiC off-axis aspheric thin-plate mirrors. The specific method is to use a medium-aperture off-axis aspheric SiC thin-plate mirror as the scaling model of an optical system mirror, to transfer the stressed mirror polishing technology used for large-aperture telescope system spliced segmented mirrors to the processing of single off-axis aspheric SiC reflection mirrors. Hence, full-aperture polishing of the off-axis aspheric SiC mirror is achieved. Further, the model parameters selected in this study can cover the stress mirror polishing technical parameters for the SiC spliced segmented mirrors of most large-aperture telescopes. With this research objective, the stress mirror polishing simulation process, mirror design, and stress loading parameter selection process for an off-axis aspheric SiC mirror were studied. On the basis of these works, the conceptual design for the stress loading equipment is presented, which then provides a basis for the development of this equipment. Finally, the conundrum that the SiC material will cost approximately five times the processing times of Zerodur [6,7] and fused quartz glass when the same mirror billet thickness is removed via annular polishing [8] and spherical polishing technology is addressed. A fast stressed mirror polishing technique based on mechanical milling and sub-aperture machining that can provide a feasible solution for the design and rapid manufacture of off-axis aspheric SiC thin-plate mirrors is presented.

2. Physical foundation and simulation process of stressed mirror polishing on SiC

High-quality asymmetric optical surfaces are relatively difficult to manufacture than axisymmetric surfaces. Several difficulties are involved in axisymmetric surface fabrication: spherical surfaces are the easiest to manufacture, while coaxial paraboloids and hyperboloids are more difficult. Despite the aid of CCOS technology, the polishing of an asymmetrical surface remains a difficult task. Stressed mirror polishing technology is an optical manufacturing technique that reduces the difficulty of polishing an asymmetric mirror to the level of polishing a spherical surface.

The principle of stressed mirror polishing is summarized as follows: (1) Based on the theoretical calculation results for small deflection deformation of an elastic thin plate, external forces are applied to a parallel thin-plate mirror blank to generate the stress distribution in the blank required so that the mirror surface deforms into an off-axis aspheric surface; this ensures that that the

Optics EXPRESS

mirror blank shows a deformation response. (2) Under conditions where the deformation of the mirror blank is maintained, a spherical disc with a diameter larger than that of the mirror blank is then used to remove and polish the mirror blank, and a sphere with the same radius of curvature as the disc is then formed. (3) After removal of the external force, the required off-axis aspheric surface is obtained when the mirror blank returns to its natural state.

Next, the application of stressed mirror polishing to the processing of mirror segments for a large-aperture astronomical telescope is investigated.

Presumably, the primary mirror of the telescope uses off-axis aspheric SiC thin-plate segments as splicing units. The total aperture of the primary mirror is close to the size of its entrance pupil. With the exception of the segment mirror on the central axis, all the unit segments have a surface that is off axis to a certain degree [9]. The distribution of the splicing segments of the primary mirror for the large-aperture telescope is shown in Fig. 1.

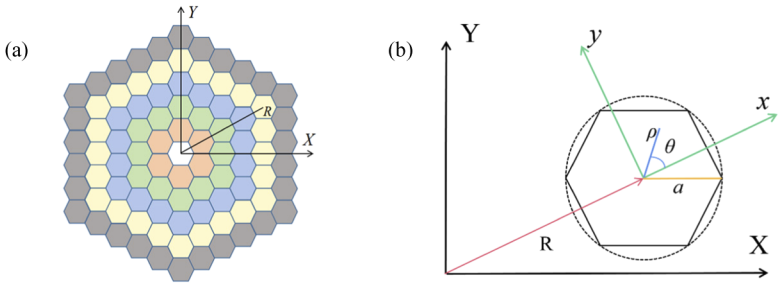

Fig. 1. Distribution of splicing segment of the primary mirror of large aperture telescope: (a) splice segment system and (b) local coordinate system on a single segment.

Suppose that the radius of the off-axis aspherical mirror is a and that the surface shape of a specific segment mirror can be expressed using the local coordinate system, as shown in Fig. 1(b). The surface shape is expressed as follows [1]:

$$Z(\rho,\theta)=\sum_{mn}\alpha_{mn}^{seg}\rho^{m}\cos(n\theta). \tag{1}$$

where m and n are integers, $m\geq n\geq 0$, and $m-n$ is an even number. Further, $\rho=(x^2+y^2)^{1/2}/a$, $\theta=\tan^{-1}(y/x)$, and α_{mn} are functional expressions for the mirror geometric parameters that are related to the off-axis quantity, aperture, cone coefficient, and radius of curvature of the mirror, respectively. The explicit equations for $\alpha seg\ mn$ are expressed as follows [1]:

$$\begin{cases}
\alpha_{20}^{seg}=\frac{a^2}{k}\left[\frac{2-K\varepsilon^2}{4(1-K\varepsilon^2)^{3/2}}\right]\\
\alpha_{22}^{seg}=\frac{a^2}{k}\left[\frac{K\varepsilon^2}{4(1-K\varepsilon^2)^{3/2}}\right]\\
\alpha_{31}^{seg}=\frac{a^3}{k^2}\left[\frac{K\varepsilon[1-(K+1)\varepsilon^2]^{1/2}(4-K\varepsilon^2)}{8(1-K\varepsilon^2)^3}\right]\\
\alpha_{33}^{seg}=\frac{a^3}{k^2}\left[\frac{K^2\varepsilon^3[1-(K+1)\varepsilon^2]^{1/2}}{8(1-K\varepsilon^2)^3}\right]\\
\alpha_{40}^{seg}=\frac{a^4}{k^3}\left[\frac{8(1+K)-24K\varepsilon^2+3K^2\varepsilon^4(1-3K)-K^3\varepsilon^6(2-K)}{64(1-K\varepsilon^2)^{9/2}}\right]\\
\alpha_{42}^{seg}=\frac{a^4}{k^3}\left[\frac{K\varepsilon^2[2(1+3K)-(9-7K)K\varepsilon^2+(2+K)K^2\varepsilon^4]}{16(1-K\varepsilon^2)^{9/2}}\right]\\
\alpha_{44}^{seg}=\frac{a^4}{k^3}\left[\frac{K^2\varepsilon^4[1+5K-K\varepsilon^2(6+5K)]}{64(1-K\varepsilon^2)^{9/2}}\right]
\end{cases}. \tag{2}$$

where $\varepsilon=R/k$, R is the off-axis quantity, k is the radius of curvature of the surface of rotation, and K is the quadric surface coefficient. Moreover, α^{seg} represents the shape coefficient of the

Optics EXPRESS

off-axis aspherical mirror of the target surface, and α^{str} represents the coefficient produced by the application of the pre-stress. The corresponding relations are listed as follows [1]:

$$\begin{cases} \alpha_{20}^{str} = a/(2k_B) - \alpha_{20}^{seg}\ (power) \\ \alpha_{22}^{str} = -\alpha_{22}^{seg}\ (astigmatism) \\ \alpha_{31}^{str} = -\alpha_{31}^{seg}\ (coma) \\ \alpha_{33}^{str} = -\alpha_{33}^{seg}\ (trefoil) \\ \alpha_{40}^{\mathrm{str}} = a^4/(8{k_B}^3) - \alpha_{40}^{seg}\ (spherical\ aberration) \\ \alpha_{42}^{str} = -\alpha_{42}^{seg}\ (secondary\ astigmatism) \\ \alpha_{44}^{str} = -\alpha_{44}^{seg}\ (quadrafoil) \end{cases} . \tag{3}$$

Here, k_B in the relations above is the segment's radius of the curvature.

The number of levers stressed by the facility is N, and the loading point is in the mirror direction θ_{n}, where $\theta_{\mathrm{n}} = 2\pi\ (n\text{-}1)/N$. The point force and moment are then expressed using the following formulas [8]:

$$\begin{cases} V(\theta_x) = V_1\cos(\theta_n) + V_2\cos(2\theta_n) \\ M(\theta_n) = M_0 + M_1\cos(\theta_n) + M_2\cos(2\theta_n) \end{cases} . \tag{4}$$

where M and V are determined by the surface shape, E is the elastic modulus of the material, ν is Poisson's ratio of the material, D is the stiffness of the plate, and h is the thickness of the mirror. These parameters are given by the following equations [8]:

$$\begin{cases} D = \frac{Eh^3}{12(1-\nu^2)} \\ M_0 = (D/a^2)[2(1+\nu)\alpha_{20}^{\mathrm{str}}] \\ M_1 = (D/a^2)[2(3+\nu)\alpha_{31}^{\mathrm{str}}] \\ M_2 = (D/a^2)[2(1-\nu)\alpha_{22}^{\mathrm{str}}] \\ V_0 = 0 \\ V_1 = -\frac{M_1}{a} \\ V_2 = \frac{2M_2}{a} \end{cases} . \tag{5}$$

From the perspective of the deformation simulation, deformation occurs between the thin plate and the target aspheric surface shape. The simulation process is shown in Fig. 2.

The simulation of the polishing method for the stress mirror polishing process was performed as follows:

(1) The spherical surface was used as the basic surface shape for the simulation, and the load parameters for the calculated values were loaded into the finite element software so that the spherical surface deformation of the finite element generated the required deviation.

(2) The surface shape of the target aspheric surface was extracted, and a virtual spherical data disk was created.

(3) To predict the final aspheric surface shape, an iterative removal condition was introduced quantitatively to remove the higher-order surface shapes generated by the deformation.

Optics EXPRESS

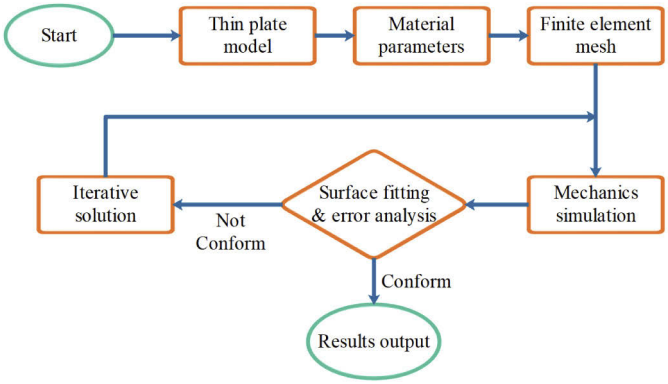

Fig. 2. Stressed mirror polishing simulation process.

The advantage of this process is that the spherical model is loaded to the aspheric surface shape, which implies that the spherical model is known and is established rapidly using MATLAB, and the verification time is then greatly reduced.

The approximate radius of the virtual data disk can be written as [1]:

$$l = l_0\left(1 + \frac{a^2}{4l_0^2}\right). \tag{6}$$

where l_0=$2k/(c + c^3)$, c = cosφ, and the slope of the x–y plane with respect to the X–Y plane is φ=tan$^{-1}\varepsilon$. The optical system parameters used in this study were derived from a scaling model of an optical system. The aspheric surface coefficient was $K = -1$, the radius of curvature of the vertex was 2032mm, the off axis was 280 mm, and the scaling factor of the optical path reduction was 4.2587.

3. Stressed mirror polishing loading point selection

In general, the experimental process of stress loading and polishing involves the processing of three low-order aberrations for astigmatism, coma, and spherical aberration, per term because these are the three main aberrations that the edge-loading technique can control. The experimental results are then compared with the model, and their repeatability is tested. However, as SiC is a brittle material with ceramic characteristics, there are numerous uncertain factors such as fracture and breakage in the stressed mirror polishing process. Traditional methods, such as calculation of the deviation quantity and verification experiments, for loading, polishing, and surface shape detection are used to approximate the target values through cyclic iterations. However, these methods are inefficient and the risk is uncontrollable. If the stress loading parameters of the SiC thin plate are provided in advance through theoretical simulations before the actual loading polishing process, the adjustments of the experimental equipment and the related waste of processing time can be avoided. This is significant for the actual machining and polishing processes.

To select the number of loading points to be used when stress loading, the merits of the different loading points should be evaluated by stress-loading the workpiece and then comparing the resulting surface errors. This paper proposes a frequency-doubling method for loading point selection that can reduce the number of attempts required to select the loading points. The following SiC thin-plate mirror dimensions were selected: 350 mm diameter, 2032 mm radius of curvature, 280 mm off axis, and 10 mm thickness. The surface shape results for 6, 12, and 24 loading points were simulated and analyzed, and the appropriate results in terms of engineering

Optics EXPRESS

cost and the technical indexes were selected. Based on the conditions described above, a single removal simulation was carried out using the MATLAB program. The sphere closest to the radius of curvature of the sphere was used as the polishing tool model, and the polishing surface model was removed. The initial single removal condition is to remove any residual surface shapes larger than 1 μm. According to the residual error results after removal, a more appropriate range of loading points is initially selected, and the surface shape results of the obtained thin-plate mirror are shown in Fig. 3.

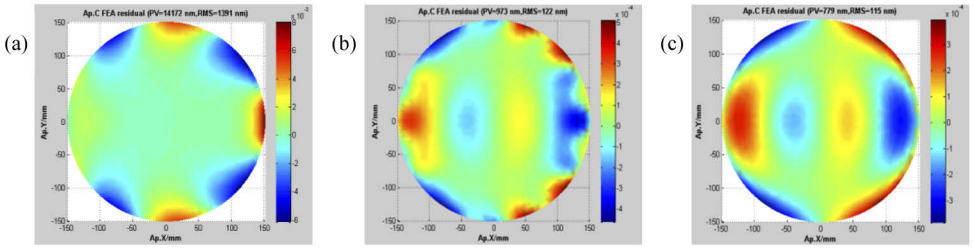

Fig. 3. Surface shapes after removal of surface residual shapes larger than 1 μm: (a) 6-point PV = 14172 nm, RMS = 1391 nm; (b) 12-point PV = 973 nm RMS = 122 nm; and (c) 24-point PV = 779 nm RMS = 115 nm.

The data in Fig. 3 show the residual differences between the resulting plane shape and the target plane shape of the finite element deformation under loading at 6, 12, and 24 points. In the case of loading at six points, the peak-valley (PV) values and root mean square (RMS) error values show major differences from the corresponding values obtained under loading at both 12 and 24 points. Thus, the six-point loading mode cannot meet the actual surface shape requirements. For further analysis, three aberrations must be compared under two loading conditions, and the results are shown in Fig. 4.

In the figure, the theoretical values represent the PV values of the lower-order quantities that constitute the plane shapes in the theoretical calculation of the full aperture. The two subsequent sets of data represent the sizes of the lower-order aberrations under the 12- and 24-point loading modes within the full aperture. The figure also shows that, after the residual removal over the full diameter, the surface shape results under the two loading modes of 12 and 24 points are close to the theoretical values. Hence, it can be assumed that, within the 350 mm diameter of the scale simulation, the two loading methods can form the shape of a predetermined paraboloid, and the differences between the two are very small. In other words, both the 12- and 24-point schemes are applicable and meet the predetermined targets in terms of their lower-order surface shape control capabilities. However, from the perspective of the complexity and rationality of the structural design, the 12-point loading mode is more suitable for the experimental scheme regarding the scaled mirror, and the 12-point loading scheme will thus be adopted in the structural design of the subsequent experimental equipment.

It should be noted that the use of 12-point loading is only a preliminary plan considering the project cost. It can be observed from Figs. 3 and 4 that although the surface shape RMS results of the 12- and 24-point loading modes are extremely similar, the residual PV value of the 12-point loading is 25% higher than that of the 24-point loading. The target value can be achieved through ion beam modification in the subsequent, or choose to remove twice, or increase the number of loading points (such as 16 or 18 points) to reduce the residual PV value. In addition, the residual PV value is related to the thickness of the mirror blank and the iterative polishing process.

Optics EXPRESS

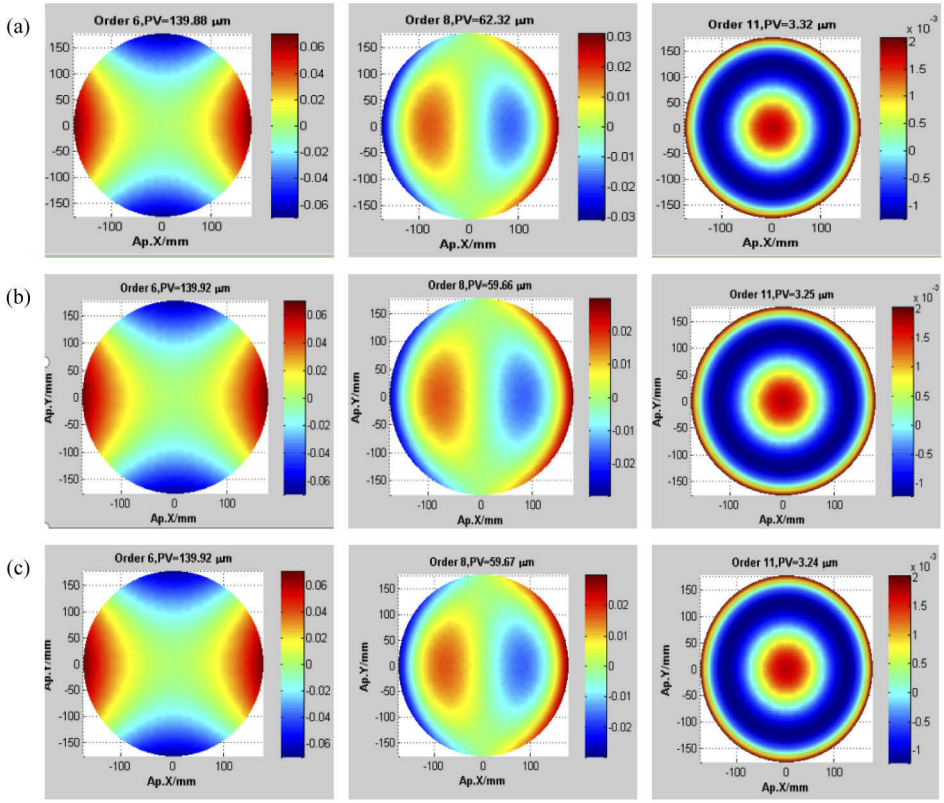

Fig. 4. Comparison of lower-order surface shapes at 12 and 24 points after removal of surface residual shapes larger than 1 μm. (a) Theoretical value of astigmatism, coma, and spherical aberration; (b) 12-point load method's value of astigmatism, coma, and spherical aberration; and (c) 24-point load method's value of astigmatism, coma, and spherical aberration.

4. Selection of SiC mirror thickness

Mirror stress is not only the result of the plane shape but also an important index to assess the performance of the SiC material. During the shear force application process, it is necessary to ensure that the mirror body stress is within the allowable range, and the upper limit for the mirror body stress is set to 150 MPa. Under a point load, the stress may exceed the SiC elastic limit because of local stress accumulation. In practice, however, the load on the rear of the mirror is in the form of pressure. In addition, the deformation stress of the mirror body decreases when the bonding area between the loading module and the rear of the mirror increases. Therefore, the

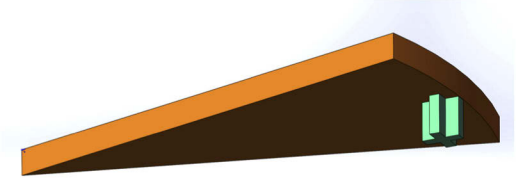

Fig. 5. 10-mm-thick SiC plate and simple loading module.

Optics EXPRESS

load is applied to simple structures to estimate the stress standard. The 10-mm-thick SiC plate and simple loading module are shown in Fig. 5.

Figure 5 shows the basic unit after connection of the loading module with the mirror body. The yellow part is the mirror body, and the green part is the loading module. It is divided by a finite element and then arranged in a circular array to form the overall structure, and the model is established. The results are shown in Fig. 6. This step provides a blueprint for the conceptual design of the loading device.

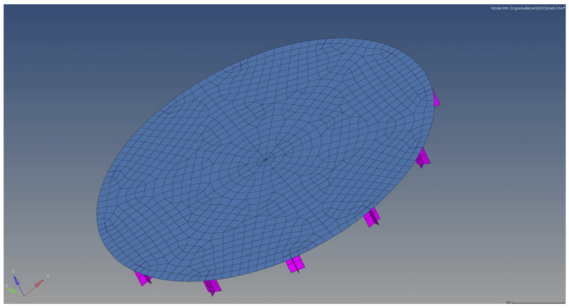

Fig. 6. Finite element division of a mirror blank with a loading module.

By applying the force and torque in the form of point loads to the center of mass of the structure, the results for the dispersed mirror stress relative to the point load are obtained. The deformation cloud diagram is shown in Fig. 7, and the maximum mirror stress is 317 MPa.

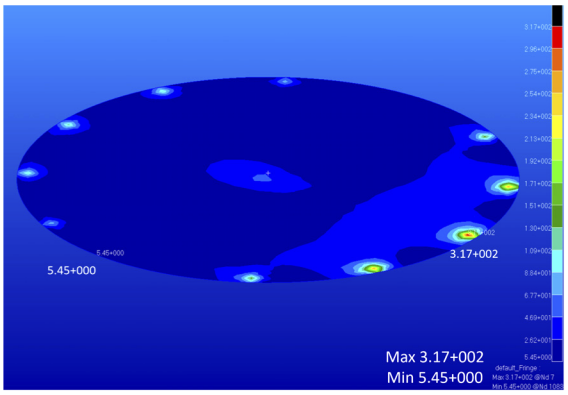

Fig. 7. Stress results for mirror body with loading module (thickness: 10 mm).

Figure 7 shows that the stress standard of the SiC mirror body with large deviations is significantly high; thus, the mirror body stress will exceed the predetermined range owing to excessive loading, even after passing through simple dispersion stress. In this study, a thickening treatment for the SiC is carried out based on the large specific stiffness characteristics and the requirement for a more stable mirror structure. Figure 8 shows the deformation cloud image for a similar structure with a thickness of 5 mm.

Figure 8 shows that the stress index of the thickened mirror body decreases significantly when the stress loading is applied relative to a body thickness of 5 mm. The figure also shows that the maximum mirror body stress is 52 MPa, which is far lower than the SiC elastic limit and, thus, meets the SiC processing requirements. However, when the mirror body thickness decreases, the effect of the removal thickness on the overall deformation also increases.

Optics EXPRESS

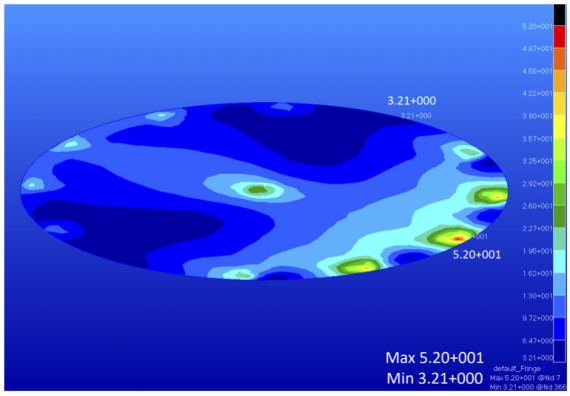

Fig. 8. Stress results for a body structure with a thickness of 5 mm.

5. Stress deformation model

Based on the results, the finite element software and the MATLAB program are used to perform virtual processing of the mirror, which allows the theoretically optimal surface shape results to be obtained rapidly. SolidWorks software was then used to build the model. The simulation material was SiC, which has an elastic modulus of 3.4×10^{11} N/m^2, Poisson's ratio of 0.16, and a thickness of 5 mm, and the mirror diameter was 350 mm. The finite element model uses Hypermesh to divide the mesh and generate the shell unit. As the model is a thin shell with parallel upper and lower surfaces, the method for extraction of the middle surface based on thin-plate approximation theory is used to establish a model with 12-point loading as an example, as shown in Fig. 9.

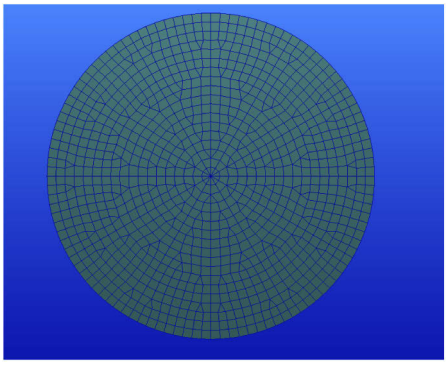

Fig. 9. Loading finite element model.

The force and moment corresponding to the application point can be obtained from Eqs. (4) and (5). The files generated by the corresponding forces and torques were then imported into Patran software and applied to the appropriate nodes to deform the mirror, thus achieving the expected aspheric surface shape. Table 1 shows the loading force and moment data corresponding to the loading at 12 points. Figure 10 shows the cloud diagram of the deformation changes after force and torque loading, and Fig. 11 shows the distorted mirror surface shape that results from the loading.

In the stressed mirror polishing simulation, it is necessary to determine a relative fixed reference position between the removal model and the disc from the perspectives of polishing efficiency

Optics EXPRESS

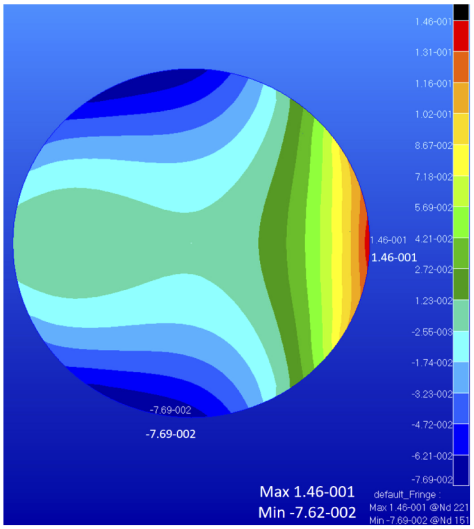

Fig. 10. Stress-loaded deformation cloud image of a 5-mm-thick SiC mirror.

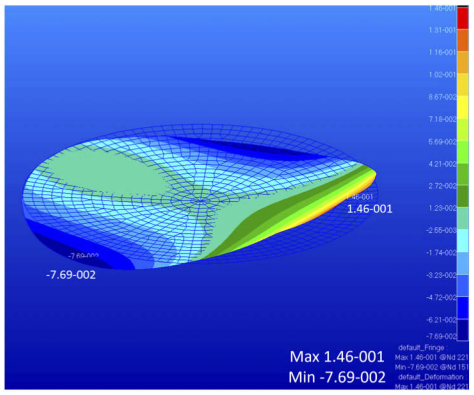

Fig. 11. Result of mirror deformation.

Table 1. Loading force and torque data at 12 points

Node	V (*x*,*y*,*z*)/N	M (*x*,*y*,*z*)
1	(0,0,-46.50)	(3555.98,-6159.13,0)
2	(0,0,-48.78)	(3257.17,-1880.53,0)
3	(0,0,-39.86)	(182.18, 0,0)
4	(0,0,-16.01)	(-1891.56,-1092.09,0)
5	(0,0,11.57)	(-1554.26,-2692.06,0)
6	(0,0,23.92)	(0,-3269.83,0)
7	(0,0,11.57)	(1554.26,-2692.06,0)
8	(0,0,-16.01)	(1891.56,-1092.09,0)
9	(0,0,-39.86)	(-182.18,0,0)
10	(0,0,-48.78)	(-3257.17,-1880.53,0)
11	(0,0,-46.50)	(-3555.98,-6159.13,0)
12	(0,0,-43.89)	(0,-8487.31,0)

Optics EXPRESS

and operability. This can be a center fixation, an edge fixation, or another location. In either case, a certain stress concentration is generated on the workpiece. When the stress is removed from the thin-plate mirror and the mirror then returns to its natural state, there will be a sudden change in shape with a large peak occurring at the original stress concentration position. This problem must be considered as part of the simulation process. In this study, the center of the mirror is selected as the overall constraint center, indicating that the stress peak caused by the loading will occur at the center of the mirror, resulting in an unnecessary deformation of the mirror. To address this problem, a uniform pressure distribution is provided on the rear of the mirror body to offset the stress at the center of the mirror body. When the pressure is loaded, the central stress is adjusted by the Patran software. When the stress is less than 10^{-2} N, the stress loading equipment structure can guarantee the required standards. As shown in Fig. 12, the stress at the mirror body center is 1.51e + 2 N without a uniform pressure distribution. Figure 13 shows the stress result at the mirror body center after the application of the uniform pressure distribution, and the stress value is 3.62e − 4 N. This forms the theoretical basis for the addition of a rubber pad between the mirror body and the back plate in the conceptual design of the stress loading equipment (see Section 6).

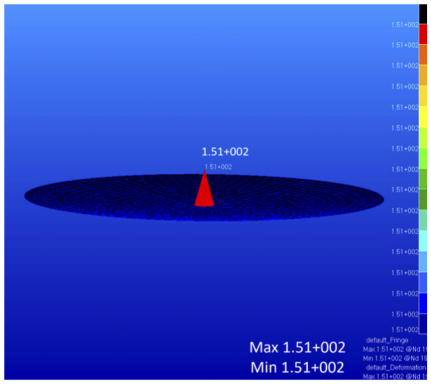

Fig. 12. Stress at the center of the mirror body without uniform pressure distribution.

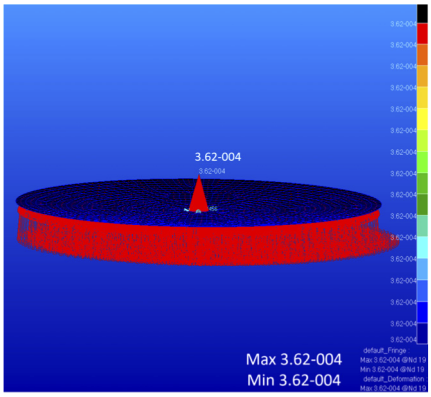

Fig. 13. Stress at the center of the mirror body after application of uniform pressure distribution.

Optics EXPRESS

Next, the SiC model is run through MATLAB procedures for the iterative removal simulation. After iterative polishing, the surface aberrations of the finite element simulation surface shapes are compared with the theoretically calculated values, and the results are shown in Fig. 14.

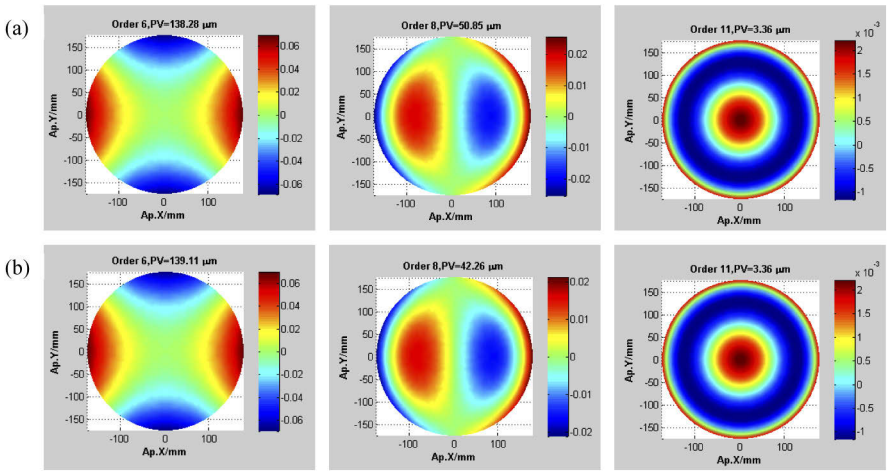

Fig. 14. Results of the surface shape and finite element surface shape for the full-caliber internal system. (a) Theoretical value of astigmatism, coma, and spherical aberration. (b) Simulation value of astigmatism, coma, and spherical aberration.

The results show that the astigmatism, coma, and spherical aberration are all in agreement with the theoretically calculated values at the full aperture. Owing to the loading mode of the stress, the edge shape variables usually exceed the theoretical deformation to ensure the overall plane shape effect. Therefore, a diameter of 300 mm was selected as the effective diameter for further comparisons. The results are shown in Fig. 15.

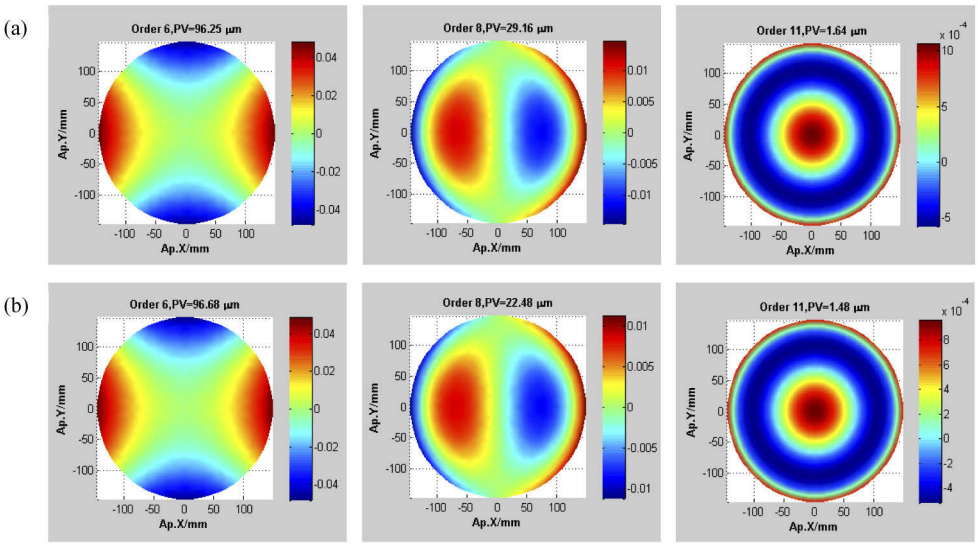

Fig. 15. Results of the surface shape and finite element surface shape for the effective caliber internal system. (a) Theoretical value of astigmatism, coma, and spherical aberration. (b) Simulation value of astigmatism, coma, and spherical aberration.

Optics EXPRESS

According to the data provided in Fig. 15, the PV values of each of the aberrations in the effective aperture decrease, and the results obtained using the SiC finite element model are actually closer to the theoretical values. Finally, the removal conditions were set by the program to remove residual values greater than 0.2 μm, and the results obtained by repeated iterations are shown in Fig. 16.

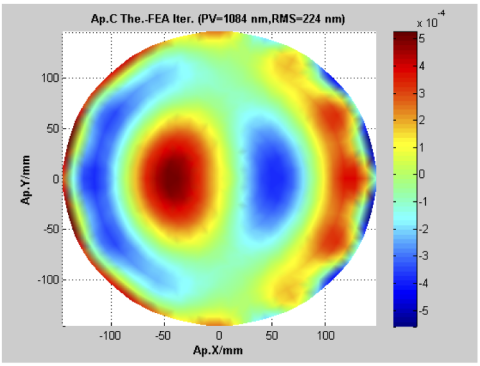

Fig. 16. Iterative polishing results for a 5-mm-thick SiC model.

As shown in Fig. 16, the RMS value of the iterative polishing residual is 0.35λ ($\lambda = 632.8$ nm), which meets the requirements of the subsequent ion beam modification process. A comparison study was conducted, and the repeated iteration results for the 10-mm-thick SiC model are shown in Fig. 17.

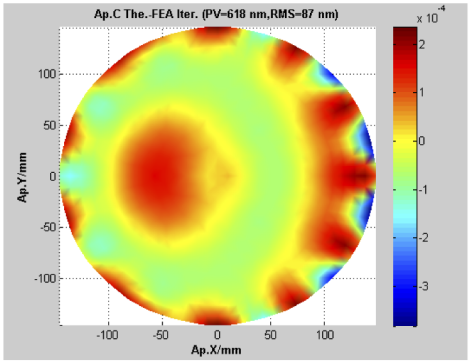

Fig. 17. Iterative polishing results for a 10-mm-thick SiC model.

From these polishing results, the iteration results for the 10-mm-thick SiC model are a PV of 618 nm and an RMS of 87 nm, while those of the 5-mm-thick SiC model are a PV of 1084 nm and an RMS of 224 nm. The reason for the differences in these results is that, although the iterative amounts removed from the two models are basically the same, the ratio of the amount removed from the thin model to the model volume is greater than the corresponding ratio for the thick model.

At this point, the advantages and disadvantages of the two thicknesses should be weighed and compared. According to the results in Figs. 7, 8, 16, and 17, the comprehensive criterion for selection of the SiC plate thickness to balance the relationship between the mirror stress and the mirror deformation is given. Based on the premise that the iterative polishing results meet their target, the thickness of the thin plate with a relatively small stress value for the mirror body is

Optics EXPRESS

selected. For example, Figs. 16 and 17 show that the iterative polishing results for the 10 mm model are better than those obtained for the 5 mm model. Figure 7 shows that the deformation force required for the 10 mm model is 300 MPa, and the mirror body may also be damaged during the polishing process. Therefore, the polishing error of the 5 mm model is larger than that of the 10 mm model, but it can also meet the requirements of the subsequent ion beam modification. However, the maximum mirror body stress of the 5 mm model is 1/6 of that of the 10 mm model. After comprehensive consideration, the 5-mm-thick SiC model was selected as the experimental model for stressed mirror polishing.

The explanation needed here is in the design and development of polishing equipment and the stressed mirror polishing experiment of a thin-plate mirror. It is necessary to conduct a simulation analysis of multiple value problems between 12- and 24-point loading and a thickness between 5 mm and 10 mm, depending on a specific situation. It is also necessary to conduct research and optimization on the relationship between the number of loading points and the allowable stress, and the relationship between the thickness and the allowable stress. This is very useful for discovering more laws and guiding engineering applications.

6. Conceptual design of stress loading equipment

As the laboratory-type stress loading equipment that uses an epitaxial loading mechanism has a simple structure and is easy to disassemble, an experimental demonstration with a medium-sized single shaft polishing machine can be performed. First, the loading structure was constructed by combining knowledge of the TMT [10], the extremely large telescope [11], and Nelson's classic work [1,2] on stressed mirror polishing while also adding a new means of simulation analysis. Based on the simulation results shown in Figs. 3–6, the structure for fixing the mirror and the loading rod with screws using connecting blocks under the mirror is adopted, as shown in Fig. 18.

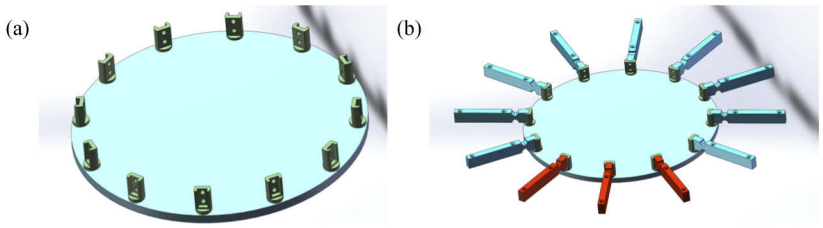

Fig. 18. Mirror with loading rod: (a) bonding module and (b) load module.

Based on the simulation results presented in Figs. 12 and 13, a rubber pad is added below the mirror to provide a uniform pressure distribution so that the stress generated at the center of the mirror is offset. The mirror supports the back plate, and the back plate is then supported by the support rod, which is connected to the back plate through the end thread to ensure overall stability, as shown in Fig. 19. This is the end of the mirror part of the experimental apparatus.

Another part of the job is to support both system construction and device integration. First, the force transducer is fixed in the corresponding fixing groove of the base using a nut. The buffer rod is then connected to the force sensor using screws. The purpose of the buffer rod's function in this case is to prevent any excessive deformation from affecting the accuracy of the measurement data of the sensor. Finally, the upper and lower parts are connected via a thread through the force application rod of the loading rod. To prevent the mirror from moving sideways during polishing, under the action of the polishing tool, a baffle guardrail can be added to the floor, as illustrated in Fig. 20.

The explanation needed here is that the above content is only the conceptual design of loading modules and devices, and a detailed design is required in a follow-up work. In the actual polishing

Optics EXPRESS

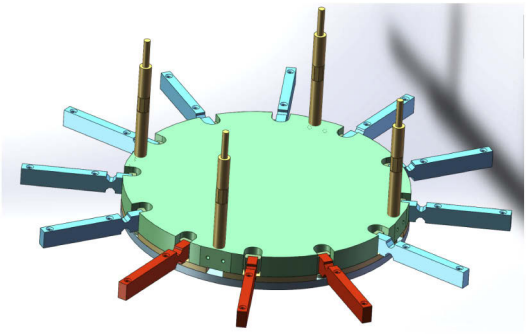

Fig. 19. Mirror body fixing module.

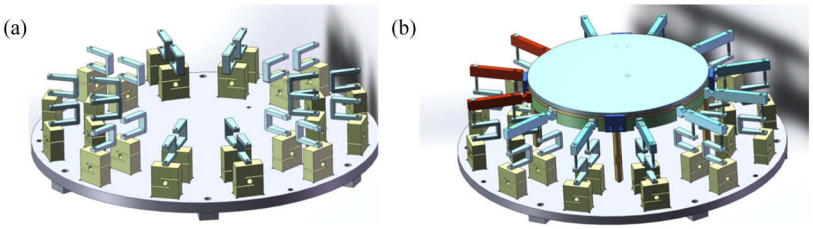

Fig. 20. Stress loading equipment: (a) force transducer installation and (b) equipment composition.

process, the center of the mirror body is not deliberately fixed, but the fixed position of the mirror body in space is completed by edge load and back support. In the polishing process, it is necessary to prevent the mirror body from moving laterally owing to the external force exerted by the polishing disk. The baffles were used on the base of the mirror body to prevent side shifting, and reaction arms [10] can also been used here. As shown in Figs. 12 and 13, in the simulation process, the stress in the center of the mirror body comes from the combined action of the loading force and the supporting force. The back support pressure was adjusted to ensure that the stress value was less than 10^{-2} N. Hence, the center constraint has almost no effect on the entire mirror body, which implies that the deviation caused by the center constraint can be ignored. Here, the rubber pad is a design in [1], but in the actual process, other means can also be selected to achieve the goal, such as the whiffle tree structure and hydraulic pad array in [10].

7. Rapid stressed mirror polishing method for SiC thin-plate submirrors

SiC is a brittle material that has ceramic characteristics. The hardness of SiC on the Mohs scale is more than 9 (that of melting quartz is 7, while that of Zerodur is 6.5), and the polishing removal rate is very low. The material removal per unit thickness produced by grinding is approximately five times longer than the same process for glass. Therefore, it is necessary to apply the stressed mirror polishing technology to the processing of the SiC thin-plate segmented mirror to address the problem of long grinding times caused by SiC's high-level hardness. This stressed mirror polishing technology has been successfully applied to the splicing of segmented mirrors for the primary mirror system of large optical telescopes. The mirror blank materials are low-expansion materials, such as Zerodur. Using annular polishing or spherical template grinding technology, the surface of the plate or other surface is machined to approximate a spherical surface after stress loading. By polishing to remove the higher-order errors after the release of the target, the off-axis aspheric surface shape can be modified for subsequent ion beams. By reducing the

Optics EXPRESS

difficulty of machining an aspheric surface to that of spherical polishing, machining efficiency is improved. This has become the mainstream mass-production technology for the splicing of segmented mirrors. For convenience of description, the two methods described above may be called the "initial plane method" and the "initial approximate spherical method," respectively. However, if the spliced segmented mirror material is replaced with SiC and the traditional "initial plane method" or the "initial approximate sphere method" is used, the extremely low removal efficiency is sufficient to offset the advantages of stressed mirror polishing.

Thus, the "initial aspheric surface method" for the rapid stressed mirror polishing of SiC thin-plate submirrors with off-axis aspheric surfaces is proposed in this study. In general, the proposed method is based on mechanical milling and sub-aperture machining technologies used in the fast stressed mirror polishing technique. The specific technical process is described as follows:

(1) The surface of the SiC thin plate to be processed is machined directly into the rough surface shape of the off-axis aspheric surface.

(2) This off-axis aspheric surface with its rough surface is then deformed and becomes a rough approximate sphere, which is close to the spherical surface under external loading, and the rough spherical surface is then polished.

(3) After the load is released, the expected off-axis aspheric surface with a smooth surface is obtained.

The advantage of this method is that it requires less material removal than the previous technique, which can improve the polishing efficiency and reduce the risk of material damage. At present, it is not difficult to mill thin SiC plates directly or process the sub-aperture into the target aspheric surface with a rough surface shape. Therefore, the implementation of the proposed "initial aspheric surface method" is feasible. However, whether the allowable stress will change after the mirror blank is processed into the initial aspheric shape is a problem that cannot be ignored in the subsequent actual processing, which requires further in-depth study.

8. Conclusion

By establishing a stress loading model of an off-axis aspheric SiC thin-plate mirror segment, a simulation analysis of full-aperture polishing of an off-axis aspheric SiC segmented mirror was performed using the finite element analysis method. The stress loading parameters, amount of material removed from the mirror, and structure data of the mirror were determined. Further, the design scheme for the corresponding stress loading equipment was presented. In terms of the manufacturing process, the concept of the "initial aspheric surface method" for the rapid stressed mirror polishing of SiC thin-plate mirrors on an off-axis aspheric surface was proposed for the first time to address various problems, such as high-level hardness, low material removal rate, and slow surface convergence of the SiC material. The results demonstrate the following. (1) When the stressed mirror polishing method is introduced into the off-axis aspheric SiC thin-plate mirror polishing process, the mechanical and optical parameters involved meet the usage requirements, and the SiC mirror blank does not have a significant evident damage risk than the other materials involved in the process. (2) The proposed "initial aspheric surface method" can be performed using a number of mature technologies in practice, and the "initial aspheric surface method and stressed mirror polishing" approach can be applied to rapid machining of the SiC thin-plate mirror segment of an off-axis aspheric surface. (3) The conceptual design of the stress loading equipment has a simple structure and is easy to use. (4) This work has reference significance for the design, development, and use of SiC thin-plate mirror stress loading equipment that is off-axis aspheric, along with the design, stressed mirror polishing, and rapid machining of these mirrors.

Optics EXPRESS

Funding

National Key Research and Development Program of China (2016YFB0500100); National Natural Science Foundation of China (11873007); National Natural Science Foundation of China (61975201).

Disclosures

The authors declare no conflicts of interest.

References

1. J. Lubliner and J. E. Nelson, "Stressed mirror polishing. 1: a technique for producing nonaxisymmetric mirrors," Appl. Opt. **19**(14), 2332–2340 (1980).
2. J. E. Nelson, G. Gabor, L. K. Hunt, J. Lubliner, and T. S. Mast, "Stressed mirror polishing. 2: fabrication of an off-axis section of a paraboloid," Appl. Opt. **19**(14), 2341–2352 (1980).
3. L. Li, D. Xue, W. Deng, X. Wang, Y. Bai, F. Zhang, and X. Zhang, "Positive dwell time algorithm with minimum equal extra material removal in deterministic optical surfacing technology," Appl. Opt. **56**(32), 9098–9104 (2017).
4. D. Wang, H. Hu, L. Li, Y. Bai, X. Luo, D. Xue, and X. Zhang, "Effects of the gap slope on the distribution of removal rate in Belt-MRF," Opt. Express **25**(22), 26600–26614 (2017).
5. H. Hu, X. Zhang, V. Ford, X. Luo, E. Qi, X. Zeng, and X. Zhang, "Edge control in a computer controlled optical surfacing process using a heterocercal tool influence function," Opt. Express **24**(23), 26809–26824 (2016).
6. R. Jedamzik, C. Kunisch, and T. Westerhoff, "ZERODUR for stress mirror polishing," Proc. SPIE **8126**, 812606 (2011).
7. R. Jedamzik, C. Kunisch, T. Westerhoff, U. Müller, and J. Daniel, "ZERODUR for stressed mirror polishing II: improved modeling of the material behavior," Proc. SPIE **8450**, 84504P (2012).
8. X. Li, Z. Jiang, X. Gong, H. Zhang, K. Chen, Y. Zheng, B. Li, B. Yu, and Q. Xu, "Stressed mirror annular polishing for scale-down TMT primary segments," Proc. SPIE **9912**, 99120A (2016).
9. T. S. Mast, J. E. Nelson, and G. E. Sommargren, "Primary mirror segment fabrication for CELT," Proc. SPIE **4003**, 43–58 (2000).
10. S. F. Sporer, "TMT: stressed mirror polishing fixture study," Proc. SPIE **6267**, 62672R (2006).
11. E. Hugot, A. Bernard, M. Laslandes, J. Floriot, T. Dufour, D. Fappani, J. M. Combes, and M. Ferrari, "Stress polishing demonstrator for ELT M1 segments and industrialization," Proc. SPIE **9145**, 914539 (2014).